Appl. Phys. A 78, 435–440 (2004)
DOI: 10.1007/s00339-003-2400-5

Applied Physics A
Materials Science & Processing

C. LUO[1]
K. REIMANN[2]
M. WOERNER[2]
T. ELSAESSER[2,✉]

Nonlinear terahertz spectroscopy of semiconductor nanostructures

[1] Department of Electrophysics, National Chiao Tung University, Hsinchu, Taiwan, R.O.C.
[2] Max-Born-Institut für Nichtlineare Optik und Kurzzeitspektroskopie, Max-Born-Str. 2A, 12489 Berlin, Germany

Received: 20 June 2003/Accepted: 18 September 2003
Published online: 14 January 2004 •

ABSTRACT Nonlinear frequency conversion and electro-optic sampling allow for the generation and phase-resolved characterization of few-cycle pulses in the frequency range up to 50 THz. Electric field transients with amplitudes of up to several MV/cm are applied to study coherent nonlinear excitations of low-dimensional semiconductors. We report the first observation of Rabi oscillations on intersubband transitions of electrons in GaAs/AlGaAs quantum wells. Frequency and phase of such oscillations are controlled in the 0.3- to 2.5-THz range via the strength and shape of the mid-infrared driving pulse.

PACS 78.67.De; 73.21.Fg; 07.57.Hm; 42.65.Re

1 Introduction

Solids display a variety of low-energy excitations which play a fundamental role in their optical and transport properties. In semiconductors, such excitations occur below the fundamental bandgap. They include degrees of freedom of the crystal lattice, e.g., acoustic and optical phonons, as well as electronic excitations such as inter-level transitions of excitons and carriers localized at impurities, intraband transitions of free electrons, inter-valence band absorptions of holes, and/or collective excitations like plasmons. In low-dimensional semiconductors, the quantum confinement of carriers leads to additional intersubband and interminiband transitions of substantial oscillator strength.

Ultrafast spectroscopy with femtosecond time resolution gives direct insight into the real-time dynamics of such excitations and thus into the microscopic interactions governing the basic nonequilibrium behavior of semiconductors [1]. Quantum coherent phenomena have received particular interest and the rapid progress of ultrafast spectroscopy has made possible highly sensitive experiments based on nonlinear coherent techniques, even for excitations with femtosecond decoherence times. Low-frequency coherence can be induced and followed in time either by nonresonant interactions with broadband optical pulses at high (optical) frequencies or by resonant interaction with ultrashort pulses in the THz frequency domain.

✉ Fax: +49-30/6392-1409, E-mail: elsasser@mbi-berlin.de

Heinrich Kurz and his coworkers have made outstanding contributions to our understanding of low-energy excitations in solids. A substantial part of their work has concentrated on the physics of coherent optical phonons. Coherent phonon oscillations which represent a nonstationary quantum coherent superposition of phonon states, were generated by excitation with broadband femtosecond pulses in the visible or near-infrared and monitored with different optical probes. In bulk GaAs [2, 3] and Ge [4, 5] as well as in thin films of $YBa_2Cu_3O_{7-\delta}$ [6], a periodic modulation of the transient reflectivity reveals the relevant phonon frequencies and picosecond dephasing times. In Te [7, 8], coherent oscillations along infrared active, i.e., non-totally symmetric phonon modes, lead to the emission of electromagnetic radiation in the frequency range around 2.5 THz. Such experiments have provided insight into the phonon generation mechanisms in the different materials and into phonon dephasing through anharmonic population relaxation and interactions with the electron-hole plasma in the sample.

Bloch oscillations in semiconductor superlattices [9–13] represent another prominent topic of Heinrich Kurz's research. Here, a coherent superposition of different states of a Wannier–Stark ladder in an electrically biased sample leads to coherent wavepacket motions of carriers. The intraband polarization originating from such oscillating wavepacket motions gives rise to coherent THz emission with a frequency depending on the electric bias of the sample in the Wannier–Stark regime [14]. This emission process allows for the generation of far-infrared pulses of nanojoule energy, which are tunable in the frequency range from 0.2 to about 10 THz [15]. The damping of the emitted electric field transients gives detailed information on the picosecond, i.e., comparably slow dephasing of the electron wavepacket by carrier-carrier scattering [15, 16]. In superlattices with a miniband width larger than the optical phonon energy, coupled Bloch-phonon oscillations were observed [17], demonstrating the pronounced resonant coupling of coherent excitations of the carrier system and the crystal lattice.

The work discussed so far was based on the generation of low-frequency quantum coherence by femtosecond broadband excitation in the visible or near-infrared spectral range. Resonant nonlinear excitation in the THz frequency range requires intense mid- and far-infrared pulses which have been generated by parametric frequency conversion. Combining

such sources with phase-resolving detection schemes, i.e., measuring transient electric fields, makes possible nonlinear coherent spectroscopy in the THz frequency range and thus opens new directions for studying low-energy excitations.

In this article, we describe a novel source for generating femtosecond THz pulses with electric field amplitudes of up to several MV/cm. Such pulses are applied to induce coherent Rabi oscillations of the intersubband polarization and population inversion in semiconductor quantum wells, i.e., to study the nonlinear THz response. We present the first observation of Rabi oscillations in which the transient optical polarization is characterized quantitatively by phase-resolved measurements of the emitted electromagnetic field.

2 Terahertz field transients with MV/cm amplitudes

There are a number of sources for ultrashort electric field transients in the THz frequency domain. In addition to optically driven antennas and striplines [18], nonlinear frequency conversion by non-phase-matched and phase-matched optical rectification represents a reliable method of THz generation. In such schemes, frequency components from the broad spectrum of a femtosecond pulse are mixed in a medium with a non-vanishing second order nonlinearity to generate electric field transients at the difference frequency [19–25]. Using input pulses of sub-30-fs duration, the frequency range up to 50 THz is covered by this technique. The maximum field amplitude of the THz transient is limited to $\leq 10\,\mathrm{kV/cm}$ for near-infrared input pulses from mode-locked Ti:sapphire oscillators. Much higher field amplitudes are possible if amplified pulses drive the frequency conversion process.

For a full, i.e., phase-resolved characterization of the electric field transients, electro-optic sampling is a particularly powerful method [26]. The time-dependent electric field is reconstructed from the polarization change of a short probe pulse in an electro-optic crystal subject to the THz field. Probe pulses shorter than half the oscillation period of the transient are required for measuring the momentary field amplitude with reasonable accuracy, a condition which is difficult to fulfill with amplified probe pulses. To overcome this problem, we recently developed a new method in which intense THz transients derived from amplified pulses are characterized with the help of synchronized probe pulses from the oscillator of the laser system [27]. This approach combines the advantages of oscillator pulses, namely short pulse widths and very low fluctuations, with the high intensity of amplified pulses.

A schematic of the experimental setup is shown in Fig. 1. A Ti:sapphire oscillator generates 12-fs pulses which pass a pulse shaper and seed a multi-pass-amplifier system working at a 1-kHz repetition rate. The amplified pulses at 790 nm are nearly Fourier-limited with a duration of 25 fs and a pulse energy of 800 μJ. The output of the amplifier propagates unfocused through a GaSe crystal in which an ultrafast electric field transient with frequencies up to 35 THz is generated by phase-matched type-I difference frequency mixing [22, 27]. The ultrafast electric-field transient is transmitted through the sample to be studied and then focused onto a 10-μm-thick (110)-oriented ZnTe crystal. At a germanium beam splitter

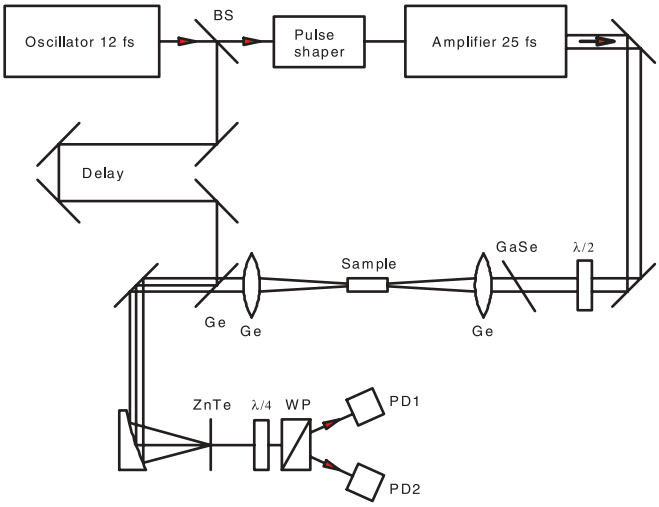

FIGURE 1 Experimental setup for the generation and measuring of THz electric field transients. BS, beam splitter, λ/4, λ/2, quarter-wave and half-wave plate, WP, Wollaston polarizer, PD1 and PD2, fast balanced photodiodes

the near-infrared probe beam is combined with the THz beam and focused onto the same position of the ZnTe crystal. The electro-optic modulation of the 12-fs probe pulse induced by the ultrafast Pockels effect results in a polarization change of the probe which is detected using a pair of fast balanced photodiodes (PD1 and PD2). By varying the time delay between the THz and the near-infrared pulses, the temporal waveform of the ultrafast electric field transient is directly sampled.

The probe beam from the Ti:sapphire oscillator has a repetition rate of 72 MHz and thus only one pulse in 72 000 coincides with an amplifier pulse. To extract the pure electro-optic signal induced by the electric field of the THz pulse we send the difference signal PD1–PD2 into two electronic gates. Gate 1 extracts the signal from the oscillator pulse in coincidence with the THz transient and gate 2 measures a reference signal using the previous oscillator pulse. For each single shot this reference is subtracted from the actual signal before averaging, eliminating deviations from a perfect intensity balance between PD1 and PD2.

In a previous study [27], we presented THz transients generated without the pulse shaper. Transients with center frequencies between 10 and 25 THz were generated in a 200-μm GaSe crystal. The absolute value of the electric field was derived from the pulse energy, the beam diameter of 50 μm, and the pulse duration. For comparison, the electric field was also estimated from the absolute value of the electro-optic signal, giving similar values. Maximum THz electric fields of approximately 1 MV/cm were generated, orders of magnitude higher than the field amplitude of transients generated with high-repetition rate oscillators. The corresponding pulse energies are on the order of 10 nJ. The pulse duration, which is defined as the full width at half maximum of the intensity envelope, had values of ~ 200 fs. Pulses of 60-fs duration, which corresponds to only 1.5 optical cycles within the intensity envelope, and a maximum field amplitude of 0.9 MV/cm were generated in a 30-μm-thick crystal (center frequency 20 THz). A noise analysis of the transients measured by electro-optic sampling demonstrates a timing jitter between the amplified

and the oscillator pulses of less than 1 fs. The sensitivity of the detection system is essentially shot-noise limited.

Well-defined changes of the optical phase can be imposed on the near-infrared input pulses with the help of the pulse shaper in our setup (Fig. 1) [24]. Through the frequency conversion process, such changes translate into the phase and shape of the THz transients. The pulse shaper can be used to tailor the spectrum in a way that only the parts needed for difference frequency generation are amplified. Figure 2a shows the spectrum generated by the oscillator, the filter function of the pulse shaper, and the resulting spectrum of tailored input pulses with a central dip and enhanced spectral components in the red and blue wings. The THz transient generated with this near-infrared input in a 200 μm thick GaSe crystal is presented in Fig. 2b. The difference signal from the two balanced photodiodes (left axis) is plotted as a function of the time delay between the 12-fs oscillator pulses and the THz transient. The center frequency of this transient is 25 THz. The electric field reaches a maximum of approximately 2 MV/cm, the highest field generated with our technique so far.

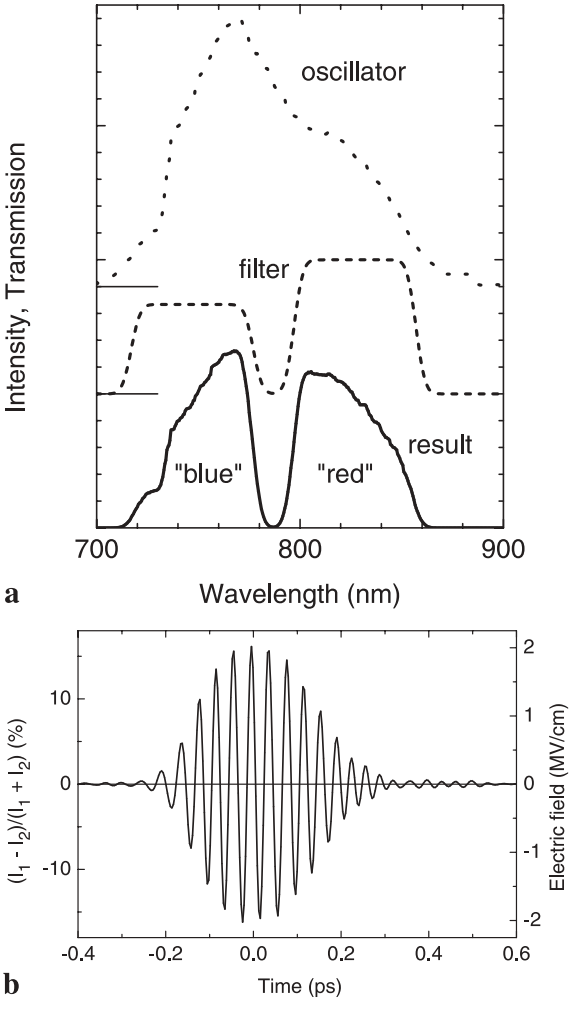

FIGURE 2 **a** Spectrum of the oscillator pulses, filter function of the pulse shaper, and resulting spectrum incident on the amplifier **b** Electric field transient generated in a 200 μm thick GaSe crystal. The center frequency of the pulse is approximately 20 THz (wavelength 15 μm), the pulse duration (FWHM of the corresponding intensity envelope) 200 fs. The electric field amplitude reaches the very high value of 2 MV/cm

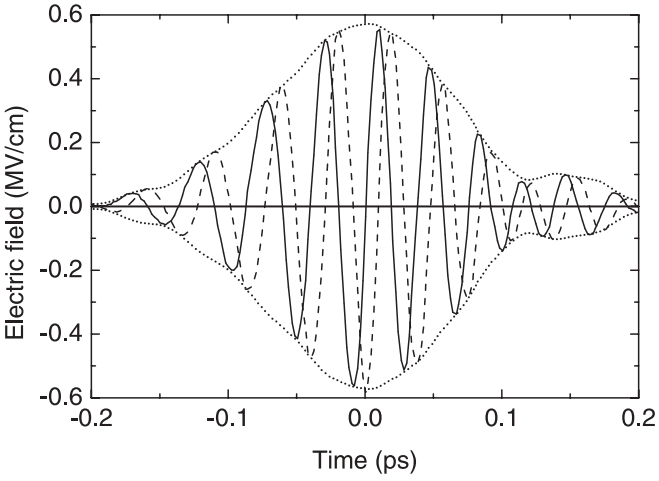

FIGURE 3 Electric field transients generated with phase-shaped input pulses in the near-infrared. The carrier-envelope phase of the THz transient is changed in a well-defined way by imposing different phases on the "red" and "blue" parts of the near-infrared pulses [see Fig. 2a] driving the generation process. The transients shown were generated in a 30 μm thick GaSe crystal with phase differences of $\pi/2$ (*solid line*) and of π (*dashed line*) between the parts of the driving pulses

Shaping the spectral phase of the input pulses also allows for changes of the carrier-envelope phase of the THz transients, as is shown in Fig. 3. The carrier-envelope phase of the THz transient is changed in a well-defined way by imposing phase differences either of $\pi/2$ or of π between the red and the blue part of the input spectrum shown in Fig. 2a. This behavior is predicted by the theory presented in [23], stating that the relative spectral phase between the extraordinary and ordinary pump beams translates directly into the carrier-envelope phase of the THz transient. Using other values of this phase shift, the carrier-envelope phase can be changed continuously. The generation of other field transients including phase-locked pulse sequences is presently under way.

3 Coherent intersubband excitations in GaAs/AlGaAs quantum wells

Semiconductor nanostructures have received much interest for optical switching as their electronic and optical properties can be tailored in a wide range by changing their nanometer dimensions. Realizing optoelectronic functions in which the phase of the electromagnetic field carries information calls for new schemes to generate, measure and control coherent optical polarizations within the short decoherence times in solid state systems.

Optical transitions resonantly driven by a coherent electromagnetic field of (carrier) frequency ω and amplitude E give rise to Rabi oscillations of the polarization amplitude and the population inversion between the optically coupled states with a frequency $\Omega = dE/\hbar$ (d: optical dipole moment) [28]. In atomic and molecular systems with comparably long decoherence times, the population inversion measured as a function of the so-called pulse area $\Theta = \frac{d\pi}{2\hbar} \int |E(t)| \, \mathrm{d}t$ displays Rabi oscillations which are accounted for by the optical Bloch equations [29] for independent two-level atoms [30, 31]. First measurements of Rabi oscillations in two- and three-dimensional semiconductors [32–35] suffer from the relatively short valence to conduction band decoherence times

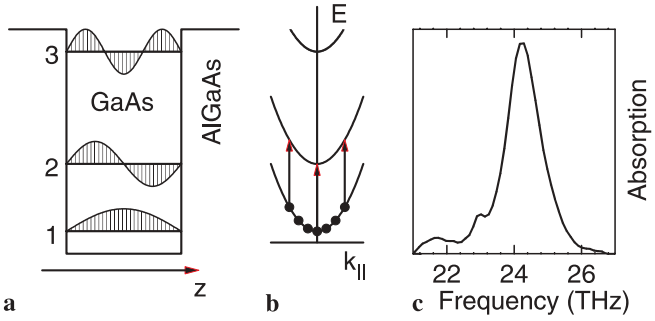

FIGURE 4 **a** Schematic of the envelope wave functions of the three lowest subbands in a quantum well **b** The dispersion parallel to the layers is nearly identical for the three subbands, so that the transition energy between two levels is independent of $\boldsymbol{k}_{\|}$ **c** Spectrum of the $1 \rightarrow 2$ intersubband absorption of the $GaAs/Al_{0.35}Ga_{0.65}As$ sample studied in our experiments, showing a line width of only 1 THz

of ~ 100 fs. In quasi-zero-dimensional semiconductor quantum dots, the substantially slower decoherence of excitonic polarizations with time constants of up to several hundreds of picoseconds has led to the recent observation of population oscillations on excitonic transitions [36, 37]. In all such cases, however, a detection of Rabi oscillations of the macroscopic polarization, a measurement of its optical phase and – in particular – an optical manipulation of the polarization amplitude have not been possible.

Intersubband transitions in quasi-two-dimensional semiconductor quantum wells represent a model system with properties favorable for implementing optical polarization control [38, 39]. The quantum confinement of the electronic wave functions along the z direction results in the formation of conduction subbands (Fig. 4). Optical transitions in the THz frequency domain occur between consecutive subbands with a very high dipole moment due to the large extension of the envelope wave functions along the z direction. The nearly parallel in-plane energy dispersion of electrons [Fig. 4b] leads to a transition energy independent of the in-plane wavevector $\boldsymbol{k}_{\|}$. As a result, well-defined narrow absorption lines are found on the $1 \rightarrow 2$ and $2 \rightarrow 3$ transitions. In Fig. 4c, the $1 \rightarrow 2$ absorption line of a high-quality n-type modulation-doped $GaAs/Al_{0.35}\ Ga_{0.65}As$ sample is shown. This sample consists of 50 GaAs quantum wells of 10-nm width separated by 20-nm wide $Al_{0.35}\ Ga_{0.65}As$ barriers. The electron density per quantum well has a value of $5 \times 10^{10}\,\mathrm{cm}^{-2}$. The properties of coherent optical polarizations on the $1 \rightarrow 2$ transition of this sample were investigated in femtosecond four-wave-mixing studies [40]. A predominant homogeneous broadening of the absorption line is found with a dephasing time of 320 fs.

In our experiments, a coherent intersubband excitation is created by a THz transient with a center frequency resonant to the $1 \rightarrow 2$ transition at 24 THz. The transmitted excitation pulse and the light emitted by the sample are measured in amplitude and phase by electro-optic sampling. Measurements were performed for different field strengths and shapes of the excitation pulses.

In Fig. 5a and c, we show – for two different intensities – the transients without the sample $E_{\mathrm{ref}}(t)$ (thin lines) and the difference between the transients with and without the sample $E_{\mathrm{diff}}(t) = E_{\mathrm{sig}}(t - \Delta t) - E_{\mathrm{ref}}(t)$ (thick lines, Δt is the delay introduced by the sample [39]). $E_{\mathrm{diff}}(t)$ is the electric field emitted by the coherent intersubband polarization $P(t)$. The data in Fig. 5a represent the linear response of the sample, which is observed for $E_{\mathrm{ref}}(0) \leq 5\,\mathrm{kV/cm}$. The re-emitted light reflects the free induction decay of the excited coherent intersubband polarization. Driven by the excitation field, a macroscopic coherent intersubband polarization $P(t)$ builds up gradually in the sample. In the case of exact resonance, this polarization is 90° out of phase with the driving field. The solution of the inhomogeneous Maxwell equations with a coherent delocalized polarization source located in a thin δ-like layer [41, 42] predicts that the re-emitted field $E(t)_{\mathrm{diff}}$ from the sample is proportional to $\partial P/\partial t$, the time derivative of $P(t)$, i.e., another 90° out of phase with $P(t)$. Both phase shifts together result in $E(t)_{\mathrm{diff}}$ being 180° out of phase with the driving field as observed in the experiment. After the driving period ($t > 0.6$ ps), $P(t)$ and concomitantly $E(t)_{\mathrm{diff}}$ decay with the dephasing time $T_2 = 320$ fs.

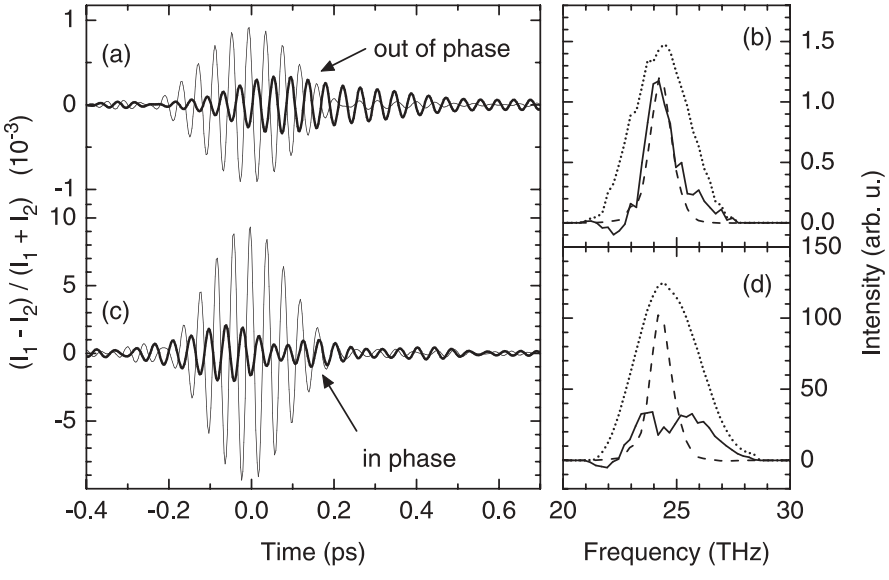

FIGURE 5 (a), (c) *Thin lines*: Input field $E_{\mathrm{ref}}(t)$ measured by ultrafast electro-optic sampling *Thick lines*: Transients of the nonlinear IS polarization given as the difference $E_{\mathrm{sig}}(t - \Delta t) - E_{\mathrm{ref}}(t)$ between the measured transients with and without sample (Δt is the delay introduced by the sample) (b), (d) Corresponding intensity spectra of $|E_{\mathrm{ref}}(\nu)|^2$ (*dotted lines*), absorbed intensity in the linear case $|E_{\mathrm{ref}}(\nu)|^2 \times [1 - T(\nu)]$ (*dashed lines*) [$T(\nu)$ is the linear transmission of the sample], and the measured nonlinearly absorbed intensity $|E_{\mathrm{ref}}(\nu)|^2 - |E_{\mathrm{sig}}(\nu)|^2$ (*solid lines*)

The time evolution of the emitted field changes drastically for large field amplitudes of the driving pulse. The data in Fig. 5c, which were taken with a driving field $E_{\mathrm{ref}}(t=0) \approx 30\,\mathrm{kV/cm}$, display a fast rise of the emitted field, a decay to zero within the driving pulse and a subsequent second emission period in which the field increases and decays again. During the first emission period, the emitted and the driving field are out of phase, similar to the linear case. In the second emission period, however, the emitted and the driving field are in phase. It is important to note that the maximum emission amplitude strongly saturates, as is evident from a comparison of Fig. 5a and c.

The results shown in Fig. 5 give direct evidence of optical Rabi oscillations which we observe for the first time directly through the nonlinear polarization, in contrast to studying the consequences of population changes. The optical Bloch equations for non-interacting two-level systems represent the most elementary approach to account for such behavior [29]. The macroscopic polarization $P(t)$, which is connected to the off-diagonal element $\varrho_{12}(t)$ of the density matrix, is described by a differential equation containing a nonlinear term that is proportional to the population inversion between the two optically coupled subbands, i.e., to the difference $(\varrho_{22} - \varrho_{11}) = (2\varrho_{22} - 1)$ of the diagonal elements of the density matrix. This nonlinear term leads (i) to a saturation of the polarization amplitude because $|\varrho_{12}(t)| \leq 1/2$ for all times t, and (ii) controls the phase of the coherent polarization generated by the driving field. For weak resonant excitation [Fig. 5a], i.e., negative population inversion and $\partial\varrho_{22}(t)/\partial t > 0$, absorption dominates. The re-emitted field $E(t)_{\mathrm{diff}} \propto \partial P(t)/\partial t$ with a phase opposite to the driving field interferes destructively with the driving field, resulting in an attenuation of the total transmitted field. For strong excitation [Fig. 5b], there is a first period in which a complete population inversion builds up $(\partial\varrho_{22}(t)/\partial t > 0)$, followed by a second period in which this inversion decreases by stimulated emission $(\partial\varrho_{22}(t)/\partial t < 0)$. Correspondingly, the emitted field and the driving field are out of phase in the first period and in phase in the second period. The amplitude of the emitted field is zero for maximum inversion, at $t = 0.08$ ps in Fig. 5b. In addition, the spectrum of the nonlinearly absorbed intensity [Fig. 5d] is much smaller than the linear absorption and shows a pronounced dip at the intersubband resonance. Thus, our data displays all the features which are indicative of intersubband Rabi flopping.

In the nonlinear regime, we performed a series of measurements with different field amplitudes of the driving pulses. In Fig. 6, the Rabi frequency as derived from the temporal envelope of the emitted field is plotted versus the maximum field amplitude of the driving pulse. The uncertainty of the electric field measurement and of the Rabi frequency is indicated by horizontal and vertical error bars, respectively. The experimental results agree reasonably well with the linear dependence expected for an electric dipole matrix element of $d = 3.7 \times 10^{-19}\,\mathrm{nm\,C}$. This value for d is obtained from the electron wave functions in the quantum well. It also reproduces the linear intersubband absorption strength of our sample.

The main features of our data are well reproduced by the optical Bloch equations as will be discussed in detail elsewhere. A full quantitative description, however, requires

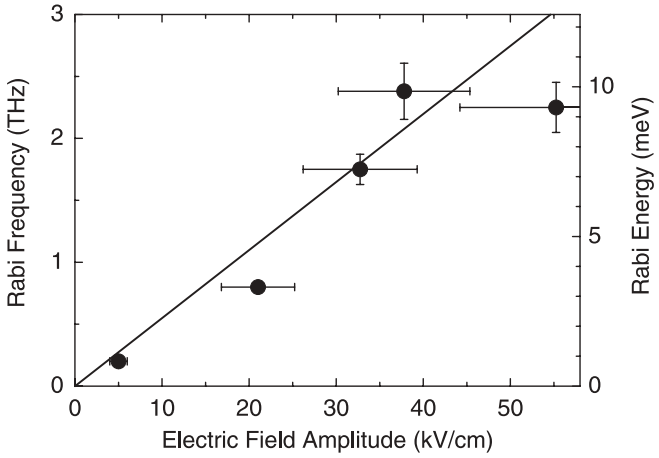

FIGURE 6 Experimentally determined Rabi frequency versus the amplitude of the incident electric-field transient (*points*) together with the expected result (*solid line*) assuming an electric-dipole matrix element of $e2.3\,\mathrm{nm} = 3.7 \times 10^{-19}\,\mathrm{nm\,C}$

the inclusion of (i) many-body effects originating from the Coulomb interactions among the quantum well electrons [43], and (ii) a possible radiative coupling of the $1 \rightarrow 2$ intersubband dipoles in different quantum wells. For the comparably low electron concentration of our sample, one expects a minor role of many-body effects for the nonlinear response, as is also suggested by our previous four-wave-mixing studies [40]. A recent theoretical analysis of intersubband absorption in this sample demonstrates that radiative damping contributes to the observed line width, i.e., it influences the measured dephasing time of 320 fs [44].

4 Conclusions

In conclusion, phase-matched optical rectification of amplified near-infrared pulses in thin GaSe crystals allows for the generation of THz pulses with field amplitudes of up to several MV/cm. The optical phase, the shape, and the duration of such pulses can be varied in a wide range by driving the frequency conversion process with phase-shaped near-infrared pulses. Phase-resolved nonlinear THz spectroscopy becomes possible by combining this THz source with a detection scheme based on electro-optic sampling. To demonstrate the potential of such techniques, we studied Rabi oscillations on intersubband transitions in n-type modulation-doped GaAs/AlGaAs quantum wells. Highly accurate measurements of the electric field emitted during and after resonant nonlinear intersubband excitation give direct evidence of Rabi oscillations of the coherent intersubband polarization. The temporal envelope and optical phase of the emitted field as well as the measured Rabi frequency are in agreement with theoretical predictions derived from the optical Bloch equations.

We envisage a broad range of further applications of the techniques presented here, including nonlinear spectroscopy of liquids and/or biological systems. With optical control of the very high electric fields at hand, ultrafast field-induced phenomena in molecules and solids may become another topic of such research.

ACKNOWLEDGEMENTS We would like to thank R. Hey and K.H. Ploog for the high-quality quantum well sample studied here and A.M. Weiner and R.P. Smith for help during the initial stages of this project. Financial support by the Deutsche Forschungsgemeinschaft is gratefully acknowledged.

REFERENCES

1 T. Elsaesser, M. Woerner: Phys. Rep. **321**, 254 (1999)
2 G.C. Cho, W. Kütt, H. Kurz: Phys. Rev. Lett. **65**, 764 (1990)
3 G.C. Cho, H.J. Bakker, T. Dekorsy, H. Kurz: Phys. Rev. B **53**, 6904 (1996)
4 T. Pfeifer, W. Kütt, H. Kurz, R. Scholz: Phys. Rev. Lett. **69**, 3248 (1992)
5 R. Scholz, T. Pfeifer, H. Kurz: Phys. Rev. B **47**, 16 229 (1993)
6 W. Albrecht, T. Kruse, H. Kurz: Phys. Rev. Lett. **69**, 1451 (1992)
7 T. Dekorsy, H. Auer, C. Waschke, H.J. Bakker, H.G. Roskos, H. Kurz, V. Wagner, P. Grosse: Phys. Rev. Lett. **74**, 738 (1995)
8 T. Dekorsy, H. Auer, H.J. Bakker, H.G. Roskos, H. Kurz: Phys. Rev. B **53**, 4005 (1996)
9 F. Bloch: Z. Phys. **52**, 555 (1928)
10 J. Bleuse, G. Bastard, P. Voisin: Phys. Rev. Lett. **60**, 2426 (1988)
11 E.E. Mendez, F. Agullo-Rueda, J.M. Hong: Phys. Rev. Lett. **60**, 2426 (1988)
12 J. Feldmann, K. Leo, J. Shah, D.A.B. Miller, J.E. Cunningham, T. Meier, G. von Plessen, A. Schulze, P. Thomas, S. Schmitt-Rink: Phys. Rev. B **46**, 7252 (1992)
13 K. Leo, P. Haring Bolivar, F. Brüggemann, R. Schwedler, K. Köhler: Solid State Commun. **84**, 943 (1992)
14 C. Waschke, H.G. Roskos, R. Schwedler, K. Leo, H. Kurz, K. Köhler: Phys. Rev. Lett. **70**, 3319 (1993)
15 R. Martini, G. Klose, H.G. Roskos, H. Kurz, H.T. Grahn, R. Hey: Phys. Rev. B **54**, 14 325 (1996)
16 P. Leisching, T. Dekorsy, H.J. Bakker, H. Kurz, K. Köhler: Phys. Rev. B **51**, 18 015 (1995)
17 T. Dekorsy, A. Bartels, H. Kurz, K. Köhler, R. Hey, K. Ploog: Phys. Rev. Lett. **85**, 1080 (2000)
18 For a review, see: D.H. Auston, in: Ultrashort Laser Pulses, W. Kaiser (Ed.), Topics in Appl. Phys., Vol. 60, Springer, Heidelberg 1993
19 S.L. Chuang, S. Schmitt-Rink, B.I. Greene, P.N. Saeta, A.F.J. Levi: Phys. Rev. Lett. **68**, 102 (1992)
20 P.C.M. Planken, M.C. Nuss, W.H. Knox, D.A.B. Miller, K.W. Goosen: Appl. Phys. Lett. **61**, 2009 (1992)
21 A. Bonvalet, M. Joffre, J.L. Martin, A. Migus: Appl. Phys. Lett. **67**, 2907 (1995)
22 R.A. Kaindl, D.C. Smith, M. Joschko, M.P. Hasselbeck, M. Woerner, T. Elsaesser: Opt. Lett. **23**, 861 (1998)
23 R.A. Kaindl, F. Eickemeyer, M. Woerner, T. Elsaesser: Appl. Phys. Lett. **75**, 1060 (1999)
24 F. Eickemeyer, R.A. Kaindl, M. Woerner, T. Elsaesser, A.M. Weiner: Opt. Lett. **25**, 1472 (2000)
25 R. Huber, A. Brodschelm, F. Tauser, A. Leitenstorfer: Appl. Phys. Lett. **76**, 3191 (2000)
26 Q. Wu, X.C. Zhang: Appl. Phys. Lett. **71**, 1285 (1997)
27 K. Reimann, R.P. Smith, A.M. Weiner, T. Elsaesser, M. Woerner: Opt. Lett. **28**, 471 (2003)
28 I.I. Rabi: Phys. Rev. **51**, 652 (1937)
29 F. Bloch: Phys. Rev. **70**, 460 (1946)
30 H.M. Gibbs: Phys. Rev. Lett. **29**, 459 (1972)
31 G.B. Hocker, C.L. Tang: Phys. Rev. Lett. **21**, 591 (1968)
32 S.T. Cundiff, A. Knorr, J. Feldmann, S.W. Koch, E.O. Göbel, H. Nickel: Phys. Rev. Lett. **73**, 1178 (1994)
33 H. Giessen, A. Knorr, S. Haas, S.W. Koch, S. Linden, J. Kuhl, M. Hetterich, M. Grün, C. Klingshirn: Phys. Rev. Lett. **81**, 4260 (1998)
34 A. Schülzgen, R. Binder, M.E. Donovan, M. Lindberg, K. Wundke, H.M. Gibbs, G. Khitrova, N. Peyghambarian: Phys. Rev. Lett. **82**, 2346 (1999)
35 O.D. Mücke, T. Tritschler, M. Wegener, U. Morgner, F.X. Kärtner: Phys. Rev. Lett. **87**, 057 401 (2001)
36 A. Zrenner, E. Beham, S. Stuffer, F. Findeis, M. Bichler, G. Abstreiter: Nature **418**, 612 (2002)
37 T.H. Stievater, Xiaoqin Li, D.G. Steel, D. Gammon, D.S. Katzer, D. Park, C. Piermarocchi, L.J. Sham: Phys. Rev. Lett. **87**, 133 603 (2001)
38 J.N. Heyman, R. Kersting, K. Unterrainer: Appl. Phys. Lett. **72**, 644 (1998)
39 F. Eickemeyer, M. Woerner, A.M. Weiner, T. Elsaesser, R. Hey, K.H. Ploog: Appl. Phys. Lett. **79**, 165 (2001)
40 R.A. Kaindl, K. Reimann, M. Woerner, T. Elsaesser, R. Hey, K.H. Ploog: Phys. Rev. B **63**, 161 308(R) (2001)
41 T. Stroucken, A. Knorr, P. Thomas, S.W. Koch: Phys. Rev. B **53**, 2026 (1996)
42 J.E. Sipe: J. Opt. Soc. Am. B **4** (1987) 481.
43 D.E. Nikonov, A. Imamoglu, L.V. Butov, H. Schmidt: Phys. Rev. Lett. **79**, 4633 (1997)
44 I. Waldmüller et al., in preparation